Solid-State ^{25}Mg NMR Spectroscopic and Computational Studies of Organic Compounds. Square-Pyramidal Magnesium(II) Ions in Aqua(magnesium) Phthalocyanine and Chlorophyll *a*

Alan Wong,[†,‡] Ramsey Ida,[†] Xin Mo,[†] Zhehong Gan,[§] Jennifer Poh,[†] and Gang Wu*[,†]

Department of Chemistry, 90 Bader Lane, Queen's University, Kingston, Ontario, Canada K7L 3N6, and Center of Interdisciplinary Magnetic Resonance, National High Magnetic Field Laboratory, 1800 East Paul Dirac Drive, Tallahassee, Florida 32310

Received: March 3, 2006; In Final Form: June 23, 2006

We report a solid-state ^{25}Mg NMR spectroscopic study of two magnesium-containing organic compounds: monopyridinated aqua(magnesium) phthalocyanine (MgPc·H_2O·Py) and chlorophyll *a* (Chl*a*). Each of these compounds contains a Mg(II) ion coordinating to four nitrogen atoms and a water molecule in a square-pyramidal geometry. Solid-state ^{25}Mg NMR spectra for MgPc·H_2O·Py were obtained at 11.7 T (500 MHz for ^{1}H) for a ^{25}Mg-enriched sample (99.1% ^{25}Mg atom) using both Hahn-echo and quadrupole Carr−Purcell Meiboom−Gill (QCPMG) pulse sequences. Solid-state ^{25}Mg NMR spectra for Chl*a* were recorded at ^{25}Mg natural abundance (10.1%) at 19.6 T (830 MHz for ^{1}H). The ^{25}Mg quadrupole parameters were determined from spectral analyses: MgPc·H_2O·Py, $C_Q = 13.0 \pm 0.1$ MHz and $\eta_Q = 0.00 \pm 0.05$; Chl*a*, $C_Q = 12.9 \pm 0.1$ MHz and $\eta_Q = 1.00 \pm 0.05$. This work represents the first time that Mg(II) ions in a square-pyramidal geometry have been characterized by solid-state ^{25}Mg NMR spectroscopy. Extensive quantum mechanical calculations for electric-field-gradient (EFG) and chemical shielding tensors were performed at restricted Hartee−Fock (RHF), density functional theory (DFT), and second-order Møller−Plesset perturbation theory (MP2) levels for both compounds. Computed ^{25}Mg nuclear quadrupole coupling constants at the RHF and MP2 levels show a reasonable basis-set convergence at the cc-pV5Z basis set (within 7% of the experimental value); however, B3LYP results display a drastic divergence beyond the cc-pVTZ basis set. A new crystal structure for MgPc·H_2O·Py is also reported.

1. Introduction

Recent developments in nuclear magnetic resonance (NMR) methodology, coupled with the availability of strong magnetic fields, have provided new possibilities for solid-state NMR studies of low-γ quadrupolar nuclei.[1,2] A particularly important trend is that solid-state NMR has emerged as a viable technique to study metal binding sites involving low-γ quadrupolar nuclei with half-integer spins such as ^{39}K (spin-3/2), ^{67}Zn (spin-5/2), and ^{25}Mg (spin-5/2) in organic and biological compounds.[3−16] These metal ions are biologically important, but technically difficult to study by NMR spectroscopy. The most reliable technique to localize these metal ions in biological macromolecules such as proteins and nucleic acids is crystallography, which can yield structural information with atomic resolution. In the meantime, it is also highly desirable to develop other spectroscopic techniques that can yield additional information about the chemical environment at the metal centers. In this regard, solid-state NMR has begun to show promise, largely because the NMR sensitivity associated with low-γ metal nuclei has been improved in recent years to a point that some important biochemical problems can be directly tackled by solid-state metal NMR. For example, Ellis and co-workers[16] have used solid-state ^{67}Zn NMR to study the nature of the ligands bound to the active Zn(II) site in human carbonic anhydrase. Their study has yielded new information about the enzymatic mechanism for this metalloenzyme. In addition to experimental solid-state ^{67}Zn NMR studies, quantum mechanical calculations have also been found useful in interpreting ^{67}Zn NMR parameters such as electric-field-gradient (EFG)[11,17] and chemical shielding tensor.[18] Wu and co-workers[14] have demonstrated that solid-state ^{39}K NMR can be used as a new probe for studying K^+ binding in DNA-related G-quadruplexes. In the context of ^{25}Mg NMR, several research groups have recently extended solid-state ^{25}Mg NMR to organic systems. Sham and Wu[6] reported solid-state ^{25}Mg NMR spectra of several Mg(II) complexes including the first ^{25}Mg multiple-quantum magic-angle spinning (MQMAS) spectrum for organic Mg(II) salts. These Mg(II) compounds were used as models for examining ^{25}Mg NMR parameters for inner-sphere Mg(II) coordination, which is a mode of Mg(II) ion binding often found in nucleic acids. Wu and co-workers have also successfully observed solid-state ^{25}Mg NMR spectra for bis(pyridine)(5,10,15,20-tetraphenylporphyrinato)magnesium(II).[13] The Mg(II) ion in this compound is coordinated to six nitrogen atoms in a distorted octahedral geometry where the ^{25}Mg quadrupole coupling constant (C_Q) exceeds 15 MHz, the largest so far being observed for all Mg(II) compounds. Frydman and co-workers studied solid-state ^{25}Mg NMR spectra for a Mg(II) salt of adenosine 5′-triphosphate (ATP).[7] Hung and Schurko reported solid-state ^{25}Mg NMR spectra for bis(cyclopentadienyl)magnesium(II).[12] These initial

* Corresponding author. E-mail: gangwu@chem.queensu.ca. Fax: 1 613 533 6669.
† Queen's University.
‡ Present address: Department of Physics, University of Warwick, Coventry, CV4 7AL, U.K.
§ National High Magnetic Field Laboratory.

10.1021/jp061350w CCC: $33.50 © 2006 American Chemical Society
Published on Web 08/02/2006

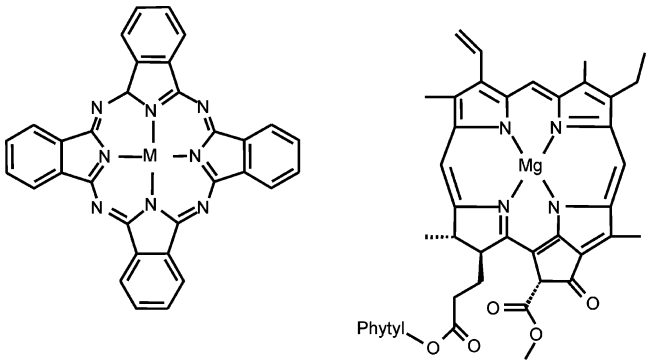

Figure 1. The chemical structures of magnesium phthalocyanine (MgPc) and chlorophyll *a* (Chl*a*).

studies demonstrate the great potential of solid-state ^{25}Mg NMR in probing the Mg(II) binding environment in organic systems. Because Mg(II) ions play pivotal roles in biological structures and functions (e.g., enzyme activity and RNA folding),[19−21] it is important to establish a baseline for the utility of solid-state ^{25}Mg NMR as an effective technique. To this end, it is necessary to characterize ^{25}Mg NMR parameters (tensors) for all known modes of Mg(II) ion binding in organic compounds. In this study, we report solid-state ^{25}Mg NMR characterization for an important class of Mg(II) ions: Mg(II) ions in a square-pyramidal geometry. The two Mg(II) compounds examined in this study (see Figure 1) are monopyridinated aqua(magnesium) phthalocyanine (MgPc·H_2O·Py) and chlorophyll *a* (Chl*a*), the most important Mg-containing compound in nature. We report results from quantum mechanical calculations on electric-field-gradient and chemical shielding tensors for these two compounds. We also report a new crystal structure for MgPc·H_2O·Py.

2. Experimental Section

Sample Preparation. 29*H*,31*H*-Phthalocycaninate (Pc, 98% purity) was obtained from Sigma-Aldrich (Ontario, Canada). ^{25}MgO (99.1% ^{25}Mg atom) was obtained from Trace Science International (Toronto, Canada). $^{25}Mg(ClO_4)_2$ was prepared by dissolving ^{25}MgO in $HClO_4$(aq) followed by evaporation to dryness. Pc and $^{25}Mg(ClO_4)_2$ were dissolved in pyridine. A few drops of water were added into the solution. The solution was gently refluxed overnight in darkness and then evaporated to dryness with a rotary evaporator. The resulting purple precipitate was then washed with cold distilled water. Purple single crystals were obtained by slow crystallization from pyridine/water in darkness at room temperature. Chl*a* was extracted from fresh spinach leaves following the literature procedure[22] with the following modification. The adsorbed pigments in the column were washed first with pure petroleum ether with the aid of pressure. This additional washing step allows removal of carotenes and much of the yellow-colored fatty material, leaving a distinct band of green chlorophylls in the upper portion of the column. Chl*a*, which appears at the lower green band in the column, was eluted with a mixture of petroleum ether and 0.5% *n*-propanol with the aid of pressure. The product was collected with a round-bottom flask covered with aluminum foil. The above procedure was repeated twice to yield 70 mg of Chl*a* from 200 g of fresh spinach leaves. UV/vis (CH_2Cl_2): Chl*a*, λ_{max} 667 and 410 nm. Solution ^{13}C and ^{1}H NMR data for Chl*a* are provided in the Supporting Information.

X-ray Crystallography. Crystallographic data for MgPc·H_2O·Py were collected from shiny red-purple hexagonal-shaped crystals with dimensions of 0.5 mm × 0.05 mm × 0.05 mm. The X-ray diffraction data were collected on a Siemens P4 single-crystal diffractometer with graphite-monochromated Mo Kα radiation operating at 50 kV and 40 mA at 180 K. Data were corrected for Lorentz and polarization effects and analyzed using Siemens SHELXTL software package.[23] The structures were solved by direct methods. Neutral atom scattering factors were taken from Cromer and Waber.[24]

Solid-State ^{25}Mg NMR. Solid-state ^{25}Mg NMR spectra at 11.75 T were recorded on a Bruker Avance-500 (11.75 T) NMR spectrometer operating at 30.62 MHz for ^{25}Mg nuclei. A Hahn-echo sequence[25] was employed to record static ^{25}Mg NMR spectra for ^{25}MgPc·H_2O·Py. The interpulse delays were set to $\tau_1 = 400$ μs and $\tau_2 = 30$ μs so that a whole echo can be acquired. The effective 90° and 180° pulses for the ^{25}Mg central transition were 1.8 and 3.6 μs, respectively. Quadrupole Carr−Purcell Meiboom−Gill (QCPMG)[26] spectra were also recorded for ^{25}MgPc·H_2O·Py at 11.75 T. The delays in the QCPMG sequence, τ_1, τ_2, τ_3, τ_4, were set to 50 μs. The spikelet separation ($1/\tau_a$) was adjusted to 10 kHz. Solid-state ^{25}Mg NMR spectra at 19.6 T were recorded at the National High Magnetic Field Laboratory (Tallahassee, FL). A Bruker Avance console and a home-built wide-line probe were used. At 19.6 T, the Larmor frequency for ^{25}Mg is 50.77 MHz. Approximately 100 mg of purified Chl*a* (as a metallic dark-green powder) was packed into a 4 mm MAS rotor. Static ^{25}Mg NMR spectra were obtained using the Hahn-echo sequence with 2.0 and 4.0 μs pulses. The B_1 field strength at the ^{25}Mg frequency was approximately 42 kHz.

Quantum Mechanical Calculations. All quantum mechanical calculations were performed using the Gaussian 03 software package[27] on a SunFire 6800 multiprocessor system (24 × 900 MHz processors and 24 GB of memory). Molecular cluster modeling was performed using SHELXTL.[23] Positions of hydrogen atoms were calculated using the standard bond distances. NMR properties were computed using various methods and basis sets to test the reliability of quantum mechanical calculations. A locally dense basis set approach was employed where various basis sets were used for the central Mg atom in combination with a 6-31G(d) basis set for all other atoms. The principal components of the electric field gradient (EFG) tensor, q_{ii} ($ii = xx, yy, zz$; $|q_{zz}| > |q_{yy}| > |q_{xx}|$ and $q_{zz} + q_{yy} + q_{xx} = 0$), were computed in atomic units (1 au = 9.717365 × 10^{21} V m^{-2}). The principal magnetic shielding tensor components (σ_{ii}) were computed with $\sigma_{iso} = (\sigma_{11} + \sigma_{22} + \sigma_{33})/3$ and $\sigma_{33} > \sigma_{22} > \sigma_{11}$. In solid-state NMR experiments for quadrupolar nuclei, the measurable quantities are quadrupole coupling constant (C_Q), asymmetry parameter (η_Q), and isotropic chemical shift (δ_{iso}). To compare calculated results with experimental NMR parameters, the following equations were used:

$$C_Q[\text{MHz}] = e^2 q_{zz} Q/h = -243.96 \times Q[\text{barn}] \times q_{zz}[\text{au}] \quad (1)$$

$$\eta_Q = (q_{xx} - q_{yy})/q_{zz} \quad (2)$$

$$\delta_{iso} = \sigma_{ref} - \sigma_{iso} \quad (3)$$

where Q is the nuclear quadrupole moment, e is the elementary charge, and h is the Planck constant, and σ_{ref} is the magnetic shielding constant for the primary chemical shift reference sample. The standard value for $Q(^{25}\text{Mg})$, 0.201 × 10^{-28} m^2, was used.[28]

TABLE 1: Crystallographic Data for MgPc·H_2O·Py

compound	MgPc·H_2O·Py
empirical formula	$C_{37}H_{23}N_9OMg$
formula weight	633.81
temperature, K	180(2)
wavelength, Å	0.710 73
crystal system	triclinic
space group	*P*1
unit cell dimensions	
a (Å)	8.823(3)
b (Å)	13.007(5)
c (Å)	14.424(6)
α (deg)	81.912(6)
β (deg)	80.385(6)
γ (deg)	74.070(7)
volume (Å^3)	1561.5(10)
Z	1
density (calculated) (g cm^{-3})	1.432
bsorption coefficient (mm^{-1})	0.109
max and min transmission	1.0000, 0.7479
crystal size (mm^3)	0.5 × 0.05 × 0.05
θ range for data collection (deg)	2.28 to 28.30
index ranges	
h	$-11 \le h \le 9$
k	$-16 \le k \le 17$
l	$-18 \le l \le 19$
reflections collected	10 459
independent reflections	6995 [R(int) = 0.0819]
completeness to	$\theta = 28.30°$ 90.1%
refinement method	full-matrix least-squares on F^2
data/restraints/parameters	6995/0/616
goodness-of-fit on F^2	0.778
final R indices [$I > 2\sigma(I)$]	$R_1 = 0.0655$, w$R_2 = 0.0931$
R indices (all data)	$R_1 = 0.2174$, w$R_2 = 0.1156$

3. Results and Discussion

3.1. Crystal Structure of MgPc·H_2O·Py. The original reason for our ^{25}MgPc·H_2O synthesis was to use this compound as a model for Chl*a*, because several MgPc·H_2O crystal structures reported in the literature[29−32] have shown that the Mg(II) ion in MgPc·H_2O is coordinated to four nitrogen atoms and one water in a square-pyramidal geometry, similar to that found in Chl*a*.[33] However, the cell dimensions determined for our sample were found to be very different from those previously reported in the literature. Because it is important to know the precise Mg coordination environment not only for interpreting solid-state NMR results but also for building a molecular model for quantum mechanical calculations, we decided to determine the complete crystal structure for our MgPc·H_2O compound. The single-crystal X-ray analysis indicates that our MgPc·H_2O crystals contain one solvent molecule of pyridine, thus the correct formula for this compound is MgPc·H_2O·Py. This monopyridinated MgPc compound has not been previously reported, despite the fact that other numbers in the series of MgPc·H_2O·Py$_x$ where $x = 0$, 2, and 3, are all known.[29−32]

MgPc·H_2O·Py crystallizes in triclinic form with a space group of *P*1 ($Z = 1$). Crystallographic data and selected structural parameters for MgPc·H_2O·Py are reported in Tables 1 and 2. A complete list of atomic coordinates for MgPc·H_2O·Py can be found in the Supporting Information. As shown in Figure 2, the Mg(II) ion in MgPc·H_2O·Py is coordinated to four nitrogen atoms from Pc and one oxygen atom from a water molecule in a square-pyramidal coordination geometry, i.e., a 4N + 1O coordination. The water molecule is further hydrogen bonded to the pyridine molecule. The Mg(II) ion is displaced by 0.447 Å from the Pc plane toward the axial water molecule. The four Mg−N bond lengths are quite similar (2.017, 2.022, 2.025, and 2.030 Å) and slightly longer than the Mg−O_W bond length, 2.002 Å. The Mg(II) ion coordination observed in MgPc·H_2O·Py is similar to that seen in the crystal structures reported previously in the literature.[29−32] The primary difference between these different crystal structures for MgPc·H_2O·Py is the packing of solvent molecules in the crystal lattice. Overall the core coordination environment at the Mg(II) center in MgPc·H_2O·Py is indeed similar to those found in chlorophyll derivatives.[33]

TABLE 2: Selected Bond Lengths (Å) and Bond Angles (deg) for MgPc·H_2O·Py[a] and Chl*a*[b]

MgPc·H_2O·Py		Chl*a*	
Mg−O1	2.002	Mg−O1	2.038
Mg−N2	2.030	Mg−N2	2.060
Mg−N4	2.017	Mg−N3	2.089
Mg−N6	2.022	Mg−N4	2.180
Mg−N8	2.025	Mg−N5	2.032
O1−Mg−N4	102.06	O1−Mg−N3	107.7
O1−Mg−N6	102.41	O1−Mg−N4	92.4
N4−Mg−N6	88.64	N3−Mg−N4	159.7
O1−Mg−N8	103.49	O1−Mg−N5	98.0
N4−Mg−N8	154.45	N3−Mg−N5	85.4
N6−Mg−N8	86.02	N4−Mg−N5	89.1
O1−Mg−N2	102.68	O1−Mg−N2	103.9
N4−Mg−N2	85.98	N3−Mg−N2	89.4
N6−Mg−N2	154.91	N4−Mg−N2	88.6
N8−Mg−N2	88.34	N5−Mg−N2	158.3

[a] This work. [b] From ref 33.

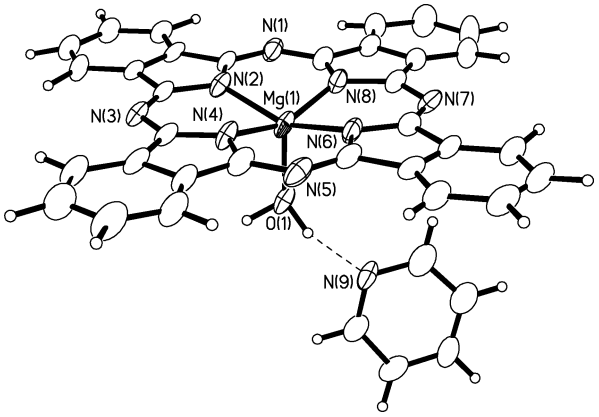

Figure 2. The molecular structure of MgPc·H_2O·Py determined by single-crystal X-ray diffraction experiment.

3.2. Solid-State ^{25}Mg NMR. Figure 3 shows the experimental and simulated static ^{25}Mg NMR spectra for ^{25}MgPc·H_2O·Py recorded at 11.75 T. The ^{25}Mg NMR signal obtained with the Hahn-echo sequence exhibits a line shape approximately 150 kHz wide. Assuming that the ^{25}Mg chemical shift anisotropy (CSA) is negligible, we obtained the ^{25}Mg nuclear quadrupole coupling constant and the asymmetry parameter for ^{25}MgPc·H_2O·Py: $C_Q = 13.0 \pm 0.1$ MHz and $\eta_Q = 0.00 \pm 0.05$. As will be discussed later, results of our magnetic shielding computation suggest that the span of the ^{25}Mg chemical shift tensor in MgPc·H_2O·Py is less than 52 ppm. Inclusion of a CSA of this magnitude and the computed tensor orientations in the NMR line shape simulation did not produce detectable difference from the one shown in Figure 3 after appropriate line broadening was applied. The ^{25}Mg QCPMG spectrum obtained for ^{25}MgPc·H_2O·Py shows a typical spikelet structure. The span of the QCPMG spectrum is in excellent agreement with that observed in the Hahn-echo spectrum. The QCPMG spectral simulation also confirms the size of the ^{25}Mg nuclear quadrupole coupling constant and the asymmetry parameter. The ^{25}Mg QCPMG experiment appears to yield a better sensitivity than the traditional Hahn-echo experiment. As seen in Figure 3, although the Hahn-echo and QCPMG spectra exhibit similar signal-to-noise ratios, the time for recording the QCPMG spectrum is approximately 3.5 times shorter than that for the Hahn-echo spectrum. In the QCPMG experiment, we collected only 15

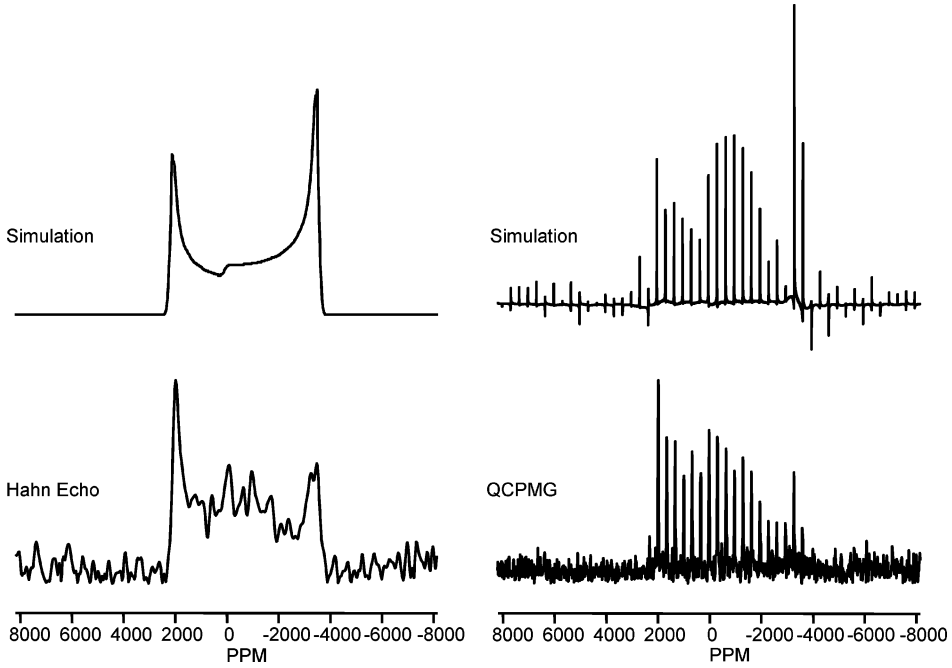

Figure 3. Experimental and simulated static ^{25}Mg NMR spectra of ^{25}MgPc·H_2O·Py at 11.75 T. The following experimental parameters were used to collect NMR data for a 40 mg sample: Hahn-echo, 0.5 MHz spectral window, 1 s recycle delay, 335 411 transients; QCPMG, 10 kHz spikelet separation, 0.5 MHz spectral window, 1 s recycle delay, and 91 826 transients.

whole echoes with a total acquisition time of 1.5 ms. Because of the crystalline nature of MgPc·H_2O·Py, the value of T_2 is relatively long, ca. 1.3 ms. Potentially, the sensitivity of the QCPMG experiment for MgPc·H_2O·Py may be further improved by collecting more echoes. We should also point out that, in both Hahn-echo and QCPMG spectra shown in Figure 3, spectral distortions do exist as a result of insufficient RF excitation. In particular, the high-frequency peak (horn) is more intense than the low-frequency one in the experimental spectra, which is opposite to that shown in the theoretical line shapes. This is because the RF transmitter was set close to 0 ppm, which is much closer to the high-frequency peak than to the low-frequency peak. Fortunately, because the ^{25}Mg nuclear quadrupole coupling constant is measured from the *positions* of these two peaks, one can still obtain reliable results from these distorted wide-line spectra.

After establishing the ^{25}Mg NMR parameters for a Mg(II) ion in a square-pyramidal geometry, we attempted to record a natural-abundance ^{25}Mg NMR spectrum for Chl*a* using both Hahn-echo and QCPMG sequences at 11.75 T. However, we were unsuccessful; acquisition for 6 days did not yield any detectable ^{25}Mg NMR signal for Chl*a*. Thus we decided to tackle this problem by using a considerably higher magnetic field. Figure 4 shows the experimental and simulated static ^{25}Mg NMR spectra for Chl*a* obtained at 19.6 T using the Hahn-echo sequence (our attempts to record a QCPMG spectrum for Chl*a* at 19.6 T have been unsuccessful). The total line width of the static ^{25}Mg NMR spectrum for Chl*a* is approximately 180 kHz, even wider than that observed for MgPc·H_2O·Py at 11.75 T. The spectral analysis yields the following parameters for Chl*a*: $C_Q = 12.9 \pm 0.1$ MHz and $\eta_Q = 1.00 \pm 0.05$. It is interesting to note that, although the value of C_Q for Chl*a* is similar to that found for MgPc·H_2O·Py, the asymmetry parameters observed for the two compounds are very different.

It may at first seem puzzling that, while MgPc·H_2O·Py and Chl*a* have essentially the same value of C_Q, the ^{25}Mg NMR spectrum observed for Chl*a* at 19.6 T exhibits, however, a larger line width (180 kHz) than that for MgPc·H_2O·Py (150 kHz)

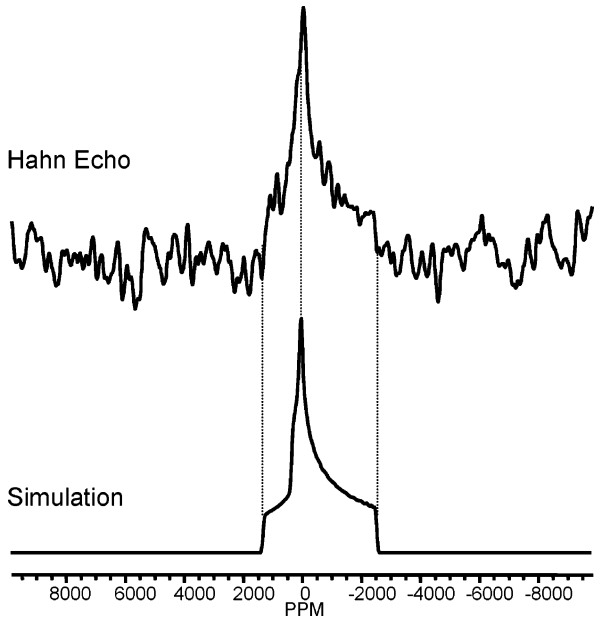

Figure 4. Experimental and simulated static ^{25}Mg NMR spectra for Chl*a* at 19.6 T. The following experimental parameters were used to collect NMR data for a 100 mg sample: 0.5 s recycle delay, 512 000 transients, and 1 MHz spectral window.

obtained at a lower field, 11.75 T. Where is the inverse B_0 scaling effect for the second-order quadrupole interaction? The explanation for these seemingly inconsistent results lies in the fact that the asymmetry parameter of the EFG tensor also plays a role in the total line width. For the central transition ($m = +1/2 \leftrightarrow -1/2$) from a half-integer spin-I nucleus, the frequency separation between the high- and low-frequency outer shoulders in the powder pattern for a stationary sample is given by[34]

$$\left(\frac{C_Q^2}{\nu_0}\right)\left(\frac{I(I+1)-(3/4)}{64I^2(2I-1)^2}\right)[(3+\eta_Q)^2+16(1+\eta_Q)] \quad (4)$$

where ν_0 is the Larmor frequency. Thus, for the same C_Q and

TABLE 3: Calculated and Experimental ^{25}Mg Nuclear Quadrupole Parameters for MgPc·H_2O and Chl*a*

basis set on Mg	RHF		B3LYP		MP2	
	C_Q/MHz	η_Q	C_Q/MHz	η_Q	C_Q/MHz	η_Q
			MgPc·H_2O			
6-31G(d)	12.598	0.090	13.332	0.088	12.622	0.091
6-311G(d)	17.400	0.075	17.806	0.064	17.479	0.076
6-311+G(d)	17.433	0.075	17.846	0.064	17.510	0.076
6-311G(3df)	17.653	0.075	17.816	0.065	17.732	0.075
6-311+G(3df)	17.666	0.075	17.846	0.065	17.744	0.075
cc-pVTZ	15.256	0.072	15.002	0.066	15.280	0.072
aug-cc-pVTZ	15.245	0.070	15.060	0.066	15.264	0.070
cc-pVQZ	14.563	0.063	17.271	0.060	14.580	0.064
aug-cc-pVQZ	14.435	0.066	18.530	0.066	14.447	0.066
cc-pV5Z	13.872	0.077	26.263	0.098	13.855	0.078
exptl	13.0 ± 0.1	0.00 ± 0.05				
			Chl*a*			
6-31G(d)	11.458	0.818	11.167	0.826	11.513	0.814
6-311G(d)	16.742	0.685	16.807	0.640	16.832	0.682
6-311+G(d)	16.769	0.685	16.847	0.639	16.858	0.681
6-311G(3df)	16.891	0.696	16.764	0.649	16.979	0.692
6-311+G(3df)	16.902	0.695	16.793	0.648	16.989	0.691
cc-pVTZ	14.345	0.702	14.093	0.654	14.466	0.697
aug-cc-pVTZ	14.348	0.701	14.174	0.651	14.466	0.696
cc-pVQZ	13.638	0.729	16.358	0.642	13.750	0.724
aug-cc-pVQZ	13.621	0.725	17.363	0.644	13.674	0.721
cc-pV5Z	13.089	0.756	27.615	0.559	13.135	0.753
exptl	12.9 ± 0.1	1.00 ± 0.05				

ν_0, the total NMR line width for $\eta_Q = 1$ is 48/25 = 1.92 times greater than that for $\eta_Q = 0$. The two compounds examined in this study represent just such extreme cases. As a result, the line narrowing effect due to the increase in B_0 (19.6/11.75 ≈ 1.67) is partially canceled by the line-width increase expected for Chl*a* where $\eta_Q = 1$, compared with MgPc·H_2O·Py where $\eta_Q = 0$.

It is also worth noting that our solid-state ^{25}Mg NMR results do not agree with those reported by Lumpkin[35] on the basis of nuclear quadrupole resonance (NQR). The reported values for C_Q(^{25}Mg) are 3.79 and 3.73 MHz for MgPc and Chl*a*, respectively. Clearly, these C_Q values are drastically different from our results. The exact reason for this discrepancy is unclear; however, Lumpkin mentioned in his paper that the nature of the axial ligands in his compounds was uncertain. In this study, we have characterized the Mg(II) coordination geometry by crystallography. In addition, as shown below, our experimental results are also in agreement with quantum mechanical calculations. Therefore, we are confident that our ^{25}Mg NMR results are correct representations for Mg(II) ions in a square-pyramidal geometry (i.e., 4N + 1O coordination).

3.3. Quantum Mechanical Calculations. Because we have obtained experimental ^{25}Mg NMR parameters for MgPc·H_2O and Chl*a*, we decided to use these data as benchmarks for testing the quality of quantum mechanical calculations in Mg-containing compounds. In a previous study, we made the first attempt to calculate ^{25}Mg NMR parameters in organic systems.[13] Here we extend our approach to examine Mg(II) ions in a square-pyramidal geometry. For MgPc·H_2O, we used the crystal structure directly to construct our molecular model. For Chl*a*, we constructed a 79-atom model using the "best set" of bond lengths and bond angles for Chl*a* derivatives reported by Kratky and Dunitz.[33] In our model for Chl*a*, the Mg atom is located above the chlorin plane by 0.39 Å. The Mg−N and Mg−O_W bond lengths are given in Table 2. Calculated results for the ^{25}Mg nuclear quadrupole and chemical shielding tensors for MgPc·H_2O and Chl*a* are summarized in Tables 3 and 4.

As illustrated in Figure 5, the computed ^{25}Mg nuclear quadrupole coupling constants show several interesting trends.

TABLE 4: Calculated ^{25}Mg Magnetic Shielding Tensors[a] for MgPc·H_2O and Chl*a*

method/basis set	σ_{iso}	σ_{11}	σ_{22}	σ_{33}	Ω^b
		MgPc·H_2O			
HF/6-31G(d)	590.8	572.3	575.7	624.3	52.0
HF/cc-pV5Z	591.6	576.4	577.6	620.8	44.4
		Chl*a*			
HF/6-31G(d)	591.4	575.3	594.2	604.6	29.3
HF/cc-pV5Z	588.2	573.2	593.3	598.1	24.9

[a] All magnetic shielding tensor components and isotropic chemical shifts are in ppm. [b] $\Omega = \sigma_{33} - \sigma_{11}$.

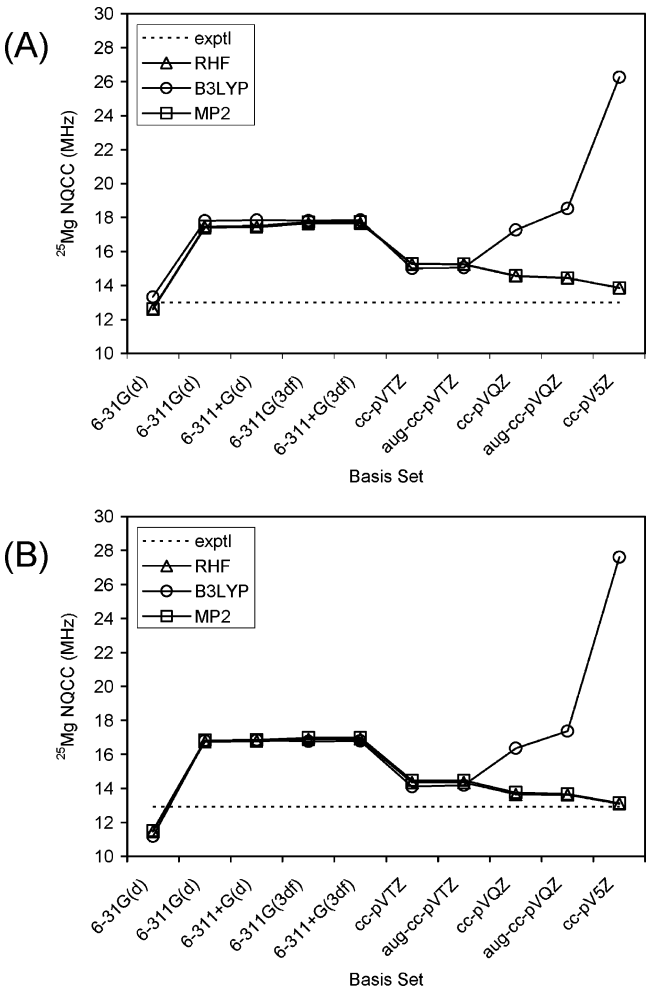

Figure 5. Basis set convergence of the computed ^{25}Mg nuclear quadrupole coupling constant for MgPc·H_2O and Chl*a*.

First, while the RHF and MP2 results converge (only higher than the experimental value by less than 1 MHz with the cc-pV5Z basis set), the B3LYP results diverge drastically from the experimental value beyond the cc-pVTZ basis set. Although the correlation consistent basis sets, cc-pVxZ where x = D(2), T(3), Q(4), 5, are known to exhibit a smooth convergence for such molecular properties as geometry and atomization energy with the hybrid B3LYP exchange functional,[36] it is apparently not the case for EFGs at the Mg nucleus in MgPc·H_2O and Chl*a*. On the other hand, there have been precedents where the hybrid B3LYP functional (and DFT in general) performs poorly for the calculations of EFGs in certain metal containing molecules.[37−39] Our finding further illustrates that caution must be exercised in computing EFG tensors at a Mg(II) center; a single-point calculation may yield unreliable results. Further studies are clearly required to see whether the same basis-set

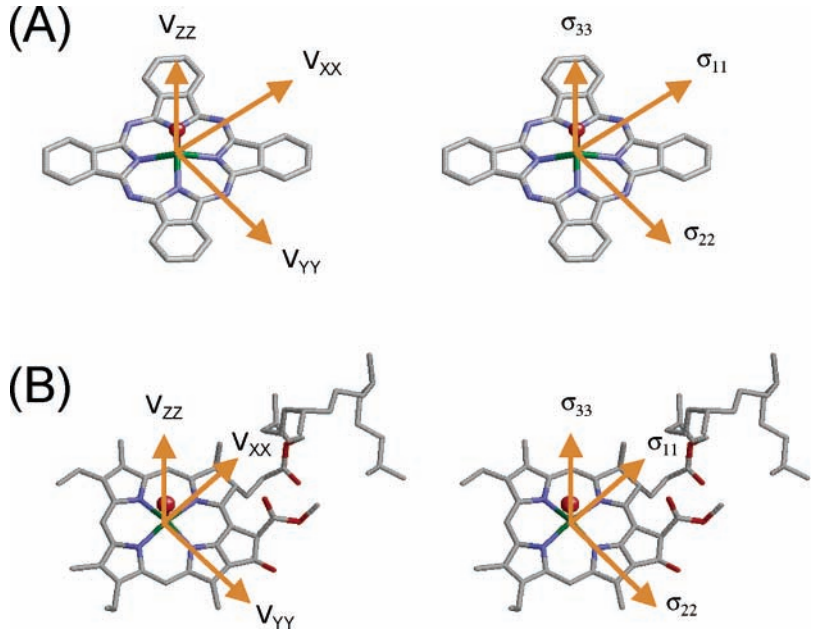

Figure 6. Calculated tensor orientations of the EFG and chemical shielding tensors in the molecular frames of (A) MgPc·H_2O and (B) Chl*a*.

divergence problem also exists for other metal centers when the hybrid B3LYP exchange functional is used. Second, the RHF and MP2 results shown in Table 3 are nearly identical, suggesting that the electron correlation effect is not important in the present system. Because the RHF calculations require only a fraction of CPU time and disk space required by the MP2 calculations, it appears that MP2 is unnecessary in EFG calculations for Mg(II) centers. Third, the observed difference in the asymmetry parameters for the two compounds ($\eta_Q = 0.0$ for MgPc·H_2O and $\eta_Q = 1.0$ for Chl*a*) is very well reproduced by the quantum mechanical calculations, providing further evidence that the computed results are reliable.

The calculated EFG tensor orientations are shown in Figure 6. For both compounds, the largest EFG tensor component, V_{ZZ}, is aligned essentially parallel to the Mg−O_W bond direction. At the HF/cc-pV5Z level, the angle between V_{ZZ} and the Mg−O_W bond is only 5.3° and 3.3° for MgPc·H_2O and Chl*a*, respectively. For MgPc·H_2O, the smallest EFG component, V_{XX}, lies approximately in the porphyrin plane, making an angle of 58.6° with respect to one of the Mg−N bonds. However, it should be noted that since the calculated EFG tensor for MgPc·H_2O is very close to axially symmetric, the difference between V_{XX} and V_{YY} is perhaps well within the computational accuracy. In contrast, the EFG tensor for Chl*a* is not axially symmetric. This can be certainly attributed to the fact that the chlorin ring in Chl*a* is nonsymmetric, i.e., three pyrrole rings and the fourth one is fused with a cyclopentanone ring. Indeed, the calculations show that V_{YY} lies along the direction connecting the Mg center with the qunioline nitrogen atom; see Figure 6. The structural basis for this EFG orientation is that the Mg−N bond length associated with the pyrrole ring fused with the cyclopentanone ring, 2.032 Å, is considerably shorter than the other two perpendicular Mg−N bonds, 2.089 and 2.180 Å. The fact that the experimental EFG tensor has exactly $\eta_Q = 1.0$ implies that the EFG along the Mg−O_W bond (2.038 Å) is equal to that along the Mg−N bond (2.032 Å) for Chl*a*. It is entirely possible then in some Chl*a* derivatives that the directions of V_{ZZ} and V_{YY} may switch as a consequence of structural perturbations either at the Mg−N bond or at the Mg−O_W bond.

As seen in Table 4, the computed ^{25}Mg chemical shielding anisotropies (CSA) for MgPc·H_2O·Py and Chl*a* are less than 52 ppm at the HF/6-31G(d) and HF/cc-pV5Z levels. The maximum line-width contribution from such a small CSA is 1.8 and 3.0 kHz at 11.75 and 19.6 T, respectively. Since the total ^{25}Mg NMR line width observed for MgPc·H_2O·Py and Chl*a* is on the order of 150−180 kHz, it is not surprising that the small ^{25}Mg CSA can be ignored in our spectral analysis. For the same reason, it was also impossible to obtain an experimentally meaningful estimate for the isotropic ^{25}Mg chemical shift for these compounds, unless very fast magic angle spinning (e.g., >50 kHz) is used. As illustrated in Figure 6, the computed ^{25}Mg chemical shift tensor orientations are similar to those for the EFG tensors in the molecular frame of reference. For both MgPc·H_2O and Chl*a*, the tensor component with the most shielding, σ_{33}, is very close to the Mg−O_W bond direction, while the other two tensor components, σ_{11} and σ_{22}, lie approximately in the porphyrin or chlorin plane. It appears that the difference in shielding tensor asymmetry for the two compounds is also consistent with the EFG results. However, because the accuracy for the ^{25}Mg chemical shielding tensor calculations has not yet been verified, further discussion is not warranted at this point.

4. Conclusion

We have obtained solid-state ^{25}Mg NMR spectra for two Mg-containing organic compounds, MgPc·H_2O·Py and Chl*a*. To the best of our knowledge, this is the first time that Mg(II) ions in a square-pyramidal geometry have been characterized by solid-state ^{25}Mg NMR spectroscopy. The large ^{25}Mg nuclear quadrupole coupling constant ($C_Q \approx 13$ MHz) associated with a square-pyramidal geometry has made direct ^{25}Mg NMR detection challenging. We have also performed extensive quantum mechanical calculations for ^{25}Mg EFG and magnetic shielding tensors at RHF, B3LYP, and MP2 levels of theory with both Pople-type and correlation consistent basis sets. The RHF and MP2 calculations show reasonable basis-set convergence with correlation consistent basis sets; with a cc-pV5Z basis set, the calculated ^{25}Mg nuclear quadrupole coupling constants for MgPc·H_2O and Chl*a* are within 7% of the experimental values. In contrast, B3LYP calculations exhibit a drastic divergence with the correlation consistent basis sets beyond the cc-pVTZ basis set. In the present systems, ^{25}Mg CSAs are too small to

be accurately measured. Our quantum mechanical calculations predict that ^{25}Mg CSA values for MgPc·H_2O·Py and Chl*a* are less than 52 ppm.

In this study we have shown that natural-abundance (10.1%) ^{25}Mg NMR detection of a single Mg(II) ion in Chl*a* (a 950 Da molecule) is possible at 19.6 T. With ^{25}Mg isotope enrichment to 99%, one gets approximately a factor of 10 in sensitivity gain, which can be translated to detection of a single Mg(II) ion from a 10 kDa molecular system without employing any other technical improvements for NMR sensitivity. If other sensitivity enhancement methods such as multiple rotor assisted population transfer or hyperbolic secant pulses (both techniques give a factor of 3−4 in sensitivity enhancement for spin-5/2 nuclei)[40,41] are combined with isotope enrichment, the molecular systems suitable for solid-state ^{25}Mg NMR can be potentially extended to >30 kDa. Another option to further improve NMR sensitivity is to use even higher magnetic fields including hybrid magnets (e.g., 40 T). We anticipate that solid-state ^{25}Mg NMR will soon find applications in both metalloenzyme chemistry and nucleic acid chemistry.

Acknowledgment. This work was supported by grants from the Natural Sciences and Engineering Research Council (NSERC) of Canada. Quantum mechanical calculations were performed at the High Performance Computing Virtual Laboratory (HPCVL) at Queen's University. We thank Dr. Ruiyao Wang for assistance in crystal structure determination and Dr. Bing Zhou for providing SIMPSON spectral simulation results.

Supporting Information Available: Complete crystal data for MgPc·H_2O·Py (seven tables and two figures) including a .CIF file. Solution ^{1}H and ^{13}C NMR spectra for Chl*a* (two figures). Cartesian coordinates for the Chl*a* model. This material is available free of charge via the Internet at http://pubs.acs.org.

References and Notes

(1) Wu, G. *Biochem. Cell Biol.* **1998**, *76*, 429.
(2) Smith, M. E. *Annu. Rep. NMR Spectrosc.* **2001**, *43*, 121.
(3) Wu, G. *Chem. Phys. Lett.* **1998**, *298*, 375.
(4) Sham, S.; Wu, G. *Can. J. Chem.* **1999**, *77*, 1782.
(5) Larsen, F. H.; Lipton, A. S.; Jakobsen, H. J.; Nielsen, N. C.; Ellis, P. D. *J. Am. Chem. Soc.* **1999**, *121*, 3783.
(6) Sham, S.; Wu, G. *Inorg. Chem.* **2000**, *39*, 4.
(7) Grant, C. V.; Frydman, V.; Frydman, L. *J. Am. Chem. Soc.* **2000**, *122*, 11743.
(8) Larsen, F. H.; Skibsted, J.; Jakobsen, H. J.; Nielsen, N. C. *J. Am. Chem. Soc.* **2000**, *122*, 7080.
(9) Lipton, A. S.; Buchko, G. W.; Sears, J. A.; Kennedy, M. A.; Ellis, P. D. *J. Am. Chem. Soc.* **2001**, *123*, 992.
(10) Lipton, A. S.; Smith, M. D.; Adams, R. D.; Ellis, P. D. *J. Am. Chem. Soc.* **2002**, *124*, 410.
(11) Lipton, A. S.; Bergquist, C.; Parkin, G.; Ellis, P. D. *J. Am. Chem. Soc.* **2003**, *125*, 3768.
(12) Hung, I.; Schurko, R. W. *Solid State Nucl. Magn. Reson.* **2003**, *24*, 78.
(13) Wu, G.; Wong, A.; Wang, S. N. *Can. J. Chem.* **2003**, *81*, 275.
(14) Wu, G.; Wong, A.; Gan, Z. H.; Davis, J. T. *J. Am. Chem. Soc.* **2003**, *125*, 7182.
(15) Wong, A.; Whitehead, R. D.; Gan, Z. H.; Wu, G. *J. Phys. Chem. A* **2004**, *108*, 10551.
(16) Lipton, A. S.; Heck, R. W.; Ellis, P. D. *J. Am. Chem. Soc* **2004**, *126*, 4735.
(17) Ida, R.; Wu, G. *J. Phys. Chem. A* **2002**, *106*, 11234.
(18) Zhang, Y.; Mukherjee, S.; Oldfield, E. *J. Am. Chem. Soc.* **2005**, *127*, 2370.
(19) *The Biological Chemistry of Magnesium*; Cowan, J. A., Ed.; Wiley: New York, 1995.
(20) Draper, D. E.; Grilley, D.; Maria Soto, A. *Annu. Rev. Biophys. Biomol. Struct.* **2005**, *34*, 221.
(21) Misra, V. K.; Draper, D. E. *Biopolymers* **1998**, *48*, 113.
(22) Strain, H. H.; Thomas, M. R.; Katz, J. J. *Biochim. Biophys. Acta* **1963**, *75*, 306.
(23) *SHELXTL Crystal Structure Analysis Package*, version 5; Bruker Analytical X-ray System, Siemens: Madison, WI, 1995.
(24) Cromer, D. T.; Waber, J. T. *International Tables for X-ray Crystallography*; Kynoch Press: Birmingham, U.K., 1974.
(25) Kunwar, A. C.; Turner, G. L.; Oldfield, E. *J. Magn. Reson.* **1986**, *69*, 124.
(26) Larsen, F. H.; Jakobsen, H. J.; Ellis, P. D.; Nielsen, N. C. *J. Phys. Chem. A* **1997**, *101*, 8597.
(27) Frisch, M. J.; Trucks, G. W.; Schlegel, H. B.; Scuseria, G. E.; Robb, M. A.; Cheeseman, J. R.; Montgomery, J. A., Jr.; Vreven, T.; Kudin, K. N.; Burant, J. C.; Millam, J. M.; Iyengar, S. S.; Tomasi, J.; Barone, V.; Mennucci, B.; Cossi, M.; Scalmani, G.; Rega, N.; Petersson, G. A.; Nakatsuji, H.; Hada, M.; Ehara, M.; Toyota, K.; Fukuda, R.; Hasegawa, J.; Ishida, M.; Nakajima, T.; Honda, Y.; Kitao, O.; Nakai, H.; Klene, M.; Li, X.; Knox, J. E.; Hratchian, H. P.; Cross, J. B.; Bakken, V.; Adamo, C.; Jaramillo, J.; Gomperts, R.; Stratmann, R. E.; Yazyev, O.; Austin, A. J.; Cammi, R.; Pomelli, C.; Ochterski, J. W.; Ayala, P. Y.; Morokuma, K.; Voth, G. A.; Salvador, P.; Dannenberg, J. J.; Zakrzewski, V. G.; Dapprich, S.; Daniels, A. D.; Strain, M. C.; Farkas, O.; Malick, D. K.; Rabuck, A. D.; Raghavachari, K.; Foresman, J. B.; Ortiz, J. V.; Cui, Q.; Baboul, A. G.; Clifford, S.; Cioslowski, J.; Stefanov, B. B.; Liu, G.; Liashenko, A.; Piskorz, P.; Komaromi, I.; Martin, R. L.; Fox, D. J.; Keith, T.; Al-Laham, M. A.; Peng, C. Y.; Nanayakkara, A.; Challacombe, M.; Gill, P. M. W.; Johnson, B.; Chen, W.; Wong, M. W.; Gonzalez, C.; Pople, J. A. *Gaussian 03*, revision C.02; Gaussian, Inc.: Wallingford CT, 2004.
(28) Pyykko, P. *Mol. Phys.* **2001**, *99*, 1617.
(29) Fisher, M. S.; Templeton, D. H.; Zalkin, A.; Calvin, M. *J. Am. Chem. Soc.* **1971**, *93*, 2622.
(30) Janczak, J.; Kubiak, R. *Polyhedron* **2001**, *20*, 2901.
(31) Janczak, J.; Idemori, Y. M. *Acta Crystallogr.* **2002**, *C58*, m549.
(32) Janczak, J.; Idemori, Y. M. *Polyhedron* **2003**, *22*, 1167.
(33) Kratky, C.; Dunitz, J. D. *J. Mol. Biol.* **1977**, *113*, 431.
(34) Stauss, G. H. *J. Chem. Phys.* **1964**, *40*, 1988.
(35) Lumpkin, O. *J. Chem. Phys.* **1975**, *62*, 3281.
(36) Wang, N. X.; Wilson, A. K. *J. Chem. Phys.* **2004**, *121*, 7632.
(37) Schwerdtfeger, P.; Pernpointner, M.; Laerdahl, J. K. *J. Chem. Phys.* **1999**, *111*, 3357.
(38) Bast, R.; Schwerdtfeger, P. *J. Chem. Phys.* **2003**, *119*, 5988.
(39) van Lenthe, E.; Baerends, E. J. *J. Chem. Phys*. **2000**, *112*, 8279.
(40) Kwak, H. T.; Prasad, S.; Clark, T.; Grandinetti, P. J. *Solid State Nucl. Magn. Reson*. **2003**, *24*, 71.
(41) Siegel, R.; Nakashima, T. T.; Wasylishen, R. E. *Chem. Phys. Lett*. **2006**, *421*, 529.